AFRL-RV-PS-
TP-2013-0008

AFRL-RV-PS-
TP-2013-0008

SOLAR Hα OSCILLATIONS FROM INTENSITY AND DOPPLER OBSERVATIONS (POSTPRINT)

Jason Jackiewicz and K. S. Balasubramaniam

01 March 2013

Technical Paper

AIR FORCE RESEARCH LABORATORY
Space Vehicles Directorate
3550 Aberdeen Ave SE
AIR FORCE MATERIEL COMMAND
KIRTLAND AIR FORCE BASE, NM 87117-5776

REPORT DOCUMENTATION PAGE

Form Approved
OMB No. 0704-0188

1. REPORT DATE *(DD-MM-YYYY)*	**2. REPORT TYPE**	**3. DATES COVERED** *(From - To)*
01-03-2013	Technical Paper	15 Jun 2010 – 30 Dec 2013

4. TITLE AND SUBTITLE
Solar Hα Oscillations From Intensity and Doppler Observations (Postprint)

5a. CONTRACT NUMBER

5b. GRANT NUMBER

5c. PROGRAM ELEMENT NUMBER
61102F

6. AUTHOR(S)
Jason Jackiewicz and K. S. Balasubramaniam

5d. PROJECT NUMBER
3001

5e. TASK NUMBER
PPM00000587

5f. WORK UNIT NUMBER
EF004376

7. PERFORMING ORGANIZATION NAME(S) AND ADDRESS(ES)
Air Force Research Laboratory
Space Vehicles Directorate
3550 Aberdeen Avenue SE
Kirtland AFB, NM 87117-5776

8. PERFORMING ORGANIZATION REPORT NUMBER
AFRL-RV-PS-TP-2013-0008

9. SPONSORING / MONITORING AGENCY NAME(S) AND ADDRESS(ES)

10. SPONSOR/MONITOR'S ACRONYM(S)
AFRL/RVBXS

11. SPONSOR/MONITOR'S REPORT NUMBER(S)

12. DISTRIBUTION / AVAILABILITY STATEMENT
Approved for public release; distribution is unlimited. (377ABW-2012-1145 dtd 28 Aug 2012)

13. SUPPLEMENTARY NOTES
This is a cleared published paper in Astrophysical Journal, Vol. 765, 1, 2013 March 1. Government Purpose Rights.

14. ABSTRACT
Chromospheric wave activity around flares and filaments has been a research focus for years, and could provide indirect measurements of local conditions that are not otherwise accessible. One interesting observed phenomenon is oscillations in filaments, activated by distant flares and the large-scale waves they produce. Characteristics of these oscillations, such as periods, amplitudes, and lifetimes, can provide unique information about the filament. We measure oscillation properties in flares and filaments from Hα chromospheric data using a new method that provides important spatial and frequency content of the dynamics. We apply the method to two flare events where filaments are observed to oscillate and determine their properties. We find strong oscillatory signal in flaring active regions in the chromosphere over a range of frequencies. Two filaments are found to oscillate without any detectable chromospheric wave acting as an activation mechanism. We find that filaments oscillate with periods of tens of minutes, but variations are significant at small spatial scales along the filamentary region. The results suggest that there is a frequency dependence of the oscillation amplitude, as well as a spatial dependence along single filaments that is more difficult to quantify. It also appears that the strength of the oscillations does not necessarily depend on the strength of the trigger, although there are other possible effects that make this conclusion preliminary. Applications of this technique to other events and different data sets will provide important new insights into the local energy densities and magnetic fields associated with dynamic chromospheric structures.

15. SUBJECT TERMS
Sun, atmosphere, filaments, prominences, flares, oscillations, Doppler velocities, chromosphere, image processing, processing

16. SECURITY CLASSIFICATION OF:			**17. LIMITATION OF ABSTRACT**	**18. NUMBER OF PAGES**	**19a. NAME OF RESPONSIBLE PERSON**
a. REPORT	**b. ABSTRACT**	**c. THIS PAGE**			K. S. Balasubramaniam
Unclassified	Unclassified	Unclassified	Unlimited	14	**19b. TELEPHONE NUMBER** *(include area code)*

The Astrophysical Journal, 765:15 (10pp), 2013 March 1 doi:10.1088/0004-637X/765/1/15

SOLAR Hα OSCILLATIONS FROM INTENSITY AND DOPPLER OBSERVATIONS

Jason Jackiewicz[1] and K. S. Balasubramaniam[2]
[1] New Mexico State University, Department of Astronomy, P.O. Box 30001, MSC 4500, Las Cruces, NM 88003, USA; jasonj@nmsu.edu
[2] Space Vehicles Directorate, Air Force Research Laboratory, Kirtland AFB, NM 87114, USA
Received 2012 October 8; accepted 2013 January 10; published 2013 February 11

ABSTRACT

Chromospheric wave activity around flares and filaments has been a research focus for years, and could provide indirect measurements of local conditions that are not otherwise accessible. One interesting observed phenomenon is oscillations in filaments, activated by distant flares and the large-scale waves they produce. Characteristics of these oscillations, such as periods, amplitudes, and lifetimes, can provide unique information about the filament. We measure oscillation properties in flares and filaments from Hα chromospheric data using a new method that provides important spatial and frequency content of the dynamics. We apply the method to two flare events where filaments are observed to oscillate and determine their properties. We find strong oscillatory signal in flaring active regions in the chromosphere over a range of frequencies. Two filaments are found to oscillate without any detectable chromospheric wave acting as an activation mechanism. We find that filaments oscillate with periods of tens of minutes, but variations are significant at small spatial scales along the filamentary region. The results suggest that there is a frequency dependence of the oscillation amplitude, as well as a spatial dependence along single filaments that is more difficult to quantify. It also appears that the strength of the oscillations does not necessarily depend on the strength of the trigger, although there are other possible effects that make this conclusion preliminary. Applications of this technique to other events and different data sets will provide important new insights into the local energy densities and magnetic fields associated with dynamic chromospheric structures.

Key words: Sun: atmosphere – Sun: filaments, prominences – Sun: flares – Sun: oscillations – techniques: image processing

Online-only material: animations, color figures

1. INTRODUCTION

It has been known for a long time (Ramsey & Smith 1966) that oscillations in solar prominences and filaments can be excited by distant flares. Such events have generally been characterized by so-called large- and small-amplitude oscillations according to the amplitude of their observed velocities (compared to the chromospheric sound and Alfvén velocities). Large-amplitude filament oscillations display speeds upward of 20 km s^{-1} and periods of tens of minutes to hours, while small-amplitude oscillations typically are a few km s^{-1}, with a less well-constrained range of periods, from minutes to hours (Arregui et al. 2012). Motions are found in both transverse and longitudinal directions with respect to the filament axis.

The chromosphere displays a wealth of wave phenomena. Early detections of oscillations in Hα measurements were carried out by Elliott (1969), and Harvey et al. (1993) used several chromospheric lines to observe the high-frequency (5 mHz) *p* modes, as well as five minute acoustic modes, both escaping from the photosphere. However, a flare (or some other source) activating a filament oscillation is a rather rare phenomenon, quite different than the oscillations that are always present in the chromosphere. Triggers of the filament activation are thought to be Moreton waves or EUV waves produced from remote flares (Eto et al. 2002; Okamoto et al. 2004; Balasubramaniam et al. 2007, 2010; Asai et al. 2012; Li & Zhang 2012), or jets and subflares (Vršnak et al. 2007), or even erupting filaments themselves (Isobe & Tripathi 2006). It is likely that intrinsic properties of the chromosphere can be deduced from studying these oscillations, as filaments seem to have associated eigenfrequencies when excited. This could be used to probe their magnetic structure and topology more precisely than traditional observations.

Recent reviews (Tripathi et al. 2009; Arregui et al. 2012) point out that much of the detailed dynamics between the interaction of the Moreton or EUV waves with the filament, the oscillatory structure (vertical/horizontal and longitudinal/transverse), the damping mechanism, and possible causes of filament eruptions are still very open issues, as these filament oscillations have only been observed in about a dozen cases.

The scope of this work is not to directly address all of the issues above, but to provide a new tool for analyzing these and similar oscillatory phenomena. We have observed two oscillating filament events: one never detected and the other previously studied by Gilbert et al. (2008). Standard analysis in previous studies typically involves reducing a three-dimensional (3D) data cube to a one-dimensional (1D) time series by spatially averaging over pixels in the filament that appear to be oscillating, and then performing a wavelet transform in time–frequency space to ascertain the variable frequency content. The reduction in dimensions has the effect of smearing possibly important spatial information. At the same time, the result may be strongly dependent on how the averaging is carried out.

Here, we describe a new technique for analyzing phenomena that have dynamic spatial and temporal scales. It is an extension of a wavelet-type technique, preserving the 3D nature of the input data. Upon application, we observe properties of chromospheric oscillations that do not easily fit into the two categories described above. We observe important differences in flaring regions and regions of oscillating filaments, indicating different responses to the trigger mechanism. We also find anomalies in oscillating filaments that have and have not interacted with a strong Moreton wave. A standard analysis is also carried out for comparison.

To introduce this technique, we first describe the example data sets in Section 2. We provide an overview of the algorithm

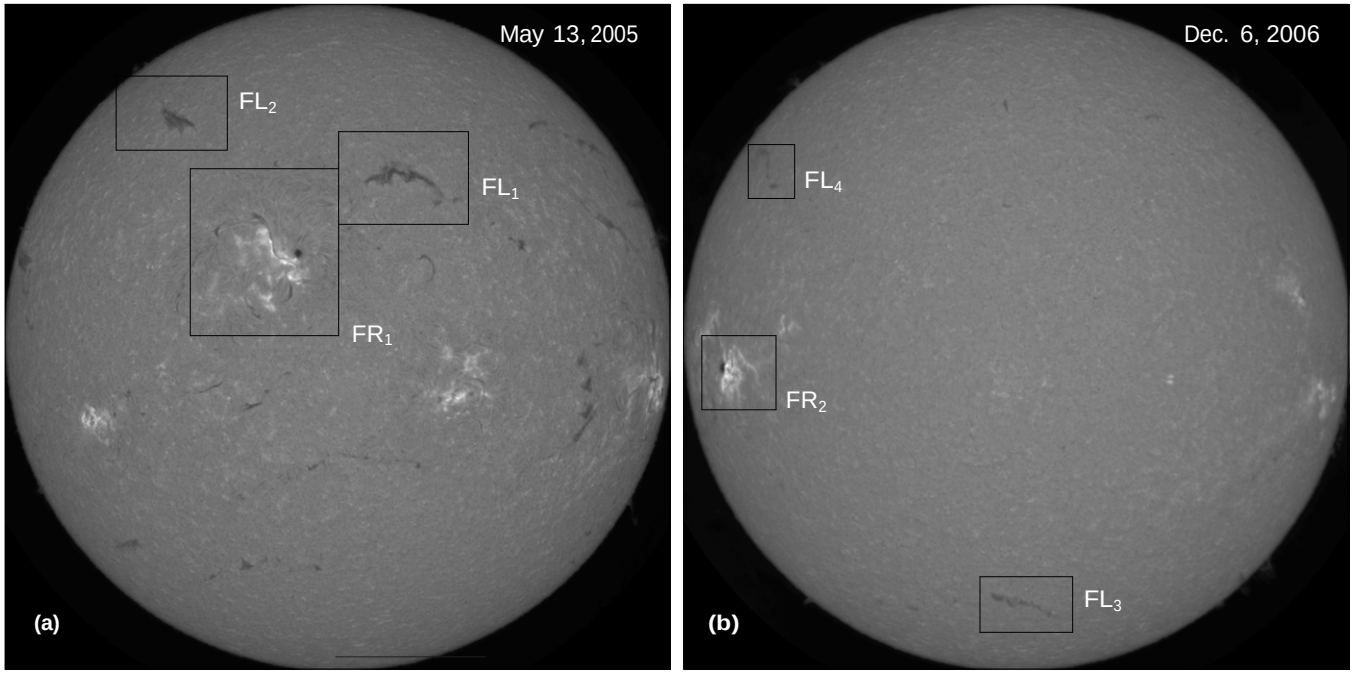

Figure 1. Snapshots (pre-flare) in Hα intensity from the ISOON telescope for the (a) 2005 M-class flare and the (b) 2006 X-class flare. Three regions of interest are marked for each event, where "FR" denotes a flaring region and "FL" denotes a filament.

(Animations of this figure are available in the online journal.)

in Section 3, which is then applied to the data and results are shown in Section 4. After comparisons of the results to standard methods and a summary are provided, a discussion is given in Section 5.

2. DATA

We study two flare events observed with the United States Air Force/National Solar Observatory Improved Solar Observing Optical Network (ISOON) telescope located at Sacramento Peak, NM (Neidig et al. 1998). Full-disk solar images (2048 × 2048 pixels at $1\overset{tt}{.}1$ sampling) at 1 minute cadence are observed in the 6563 Å Hα line center with a 0.1 Å bandpass filter. Corresponding Doppler maps are also utilized and have been constructed by the following procedure: 14 images across 14 wavelengths centered around the spectral line were gathered on a day in 2004 when there was little activity on the Sun. After calibrating the images for intensity corrections and flat-fields, spectral line profiles for each 1.1 arcsec pixel were obtained, separately. From the center-of-gravity (spectral line center) for each spectral line, the intensity difference at ± 0.4 Å, and a Doppler shift (line center for each pixel, mean line center for entire image), was measured. By plotting all of the points of Doppler shift versus the intensity difference, a characteristic relationship is found. For any day of observing the intensity differences, a conversion of that measure to Doppler shift is computed (assuming that the calibration holds true). In the flares and filaments considered here, the Hα line wings remain in absorption (Balasubramaniam et al. 2004).

A solar flare of X-ray strength M8.0 occurred on 2005 May 13 around 16:13 UT in active region NOAA 10759. It was a classic two-ribbon flare that also corresponded to a very large coronal mass ejections that delivered the most intense geomagnetic activity of 2005 (Bisi et al. 2010). Various characteristics of this well-known event have been studied (Yurchyshyn et al. 2006; Liu et al. 2007; Kazachenko et al. 2009), although this is the first time that oscillations in the active region and the nearby filaments have been detected. The second event occurred on 2006 December 6, where an X-class flare erupted at about 18:40 UT in NOAA 10930. For both cases, ISOON provided high-quality intensity and Doppler data from about four hours before until four hours after flare initiation. Pre-flare snapshots of full-disk Hα intensity images for each data set are shown in Figure 1. The flaring active regions (bright in Hα), as well as several quiescent filaments (dark in Hα) that this investigation targets, are outlined in boxes.

One important difference between these two flares is that the 2006 event produced a prominent Moreton wave (Gilbert et al. 2008; Balasubramaniam et al. 2010), a fast-moving chromospheric disturbance. This particular wave propagated from the active region and interacted with several filaments on the solar disk, some quite far from the excitation location. Filament–wave interactions in this flare were studied in detail by Gilbert et al. (2008). A second important difference is that the active region responsible for the 2006 event is located close to the limb, where strong (horizontal) velocity signals should be apparent in the line-of-sight Doppler observations.

3. DATA ANALYSIS

Studies of oscillations in filaments in the past have used velocity time series maps from both wings of a spectral line and determined when the filament transitions from redshifted to blueshifted, giving an estimation of the period (e.g., Okamoto et al. 2004; Gilbert et al. 2008). Frequency content has also been derived by spatially averaging a set of pixels in the region of interest to produce a proxy 1D "light curve," and then using wavelet techniques (Jain & Tripathy 1998; Maurya & Ambastha 2008; Pintér et al. 2008).

We demonstrate a simple and powerful way of visualizing these types of data, which preserves both frequency and spatio-temporal information. We generate what we call "frequency-filtered amplitude movies" (FFAMs), with a method similar to what would be described as 3D wavelet analysis.

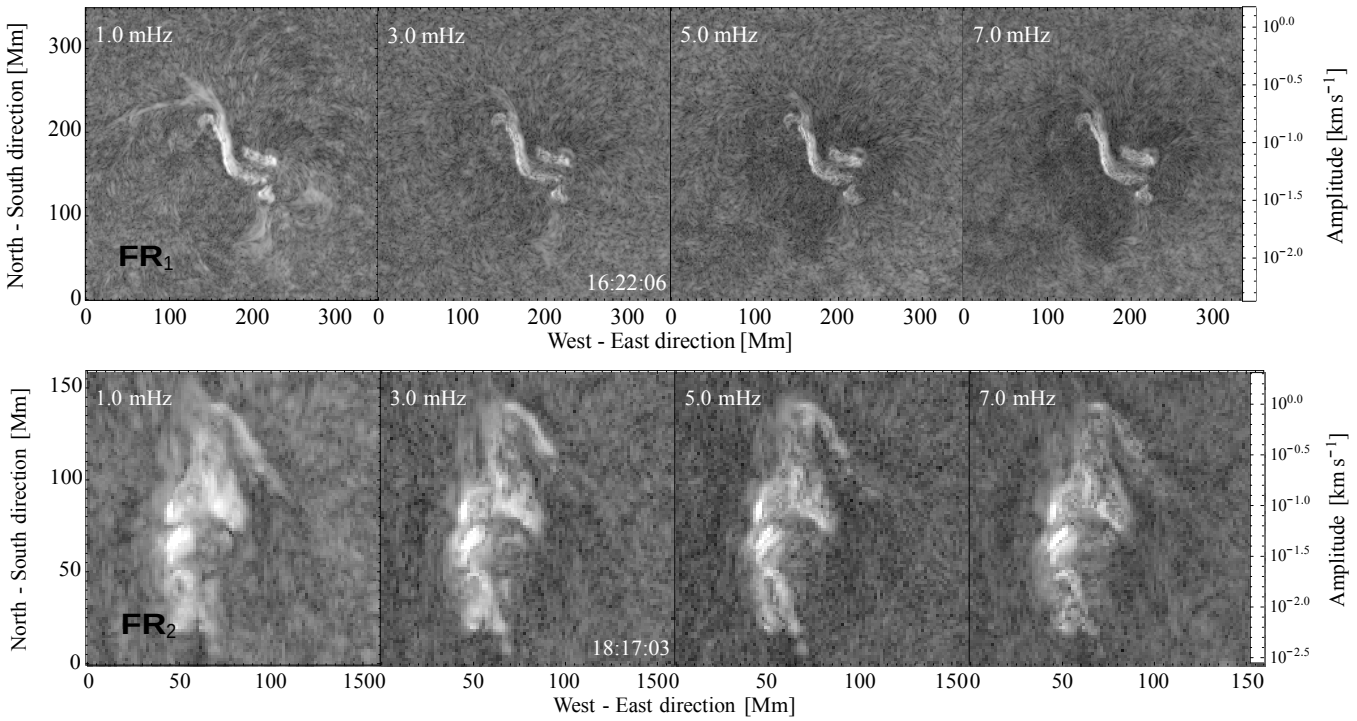

Figure 2. Two flaring regions. Each panel is a snapshot of an FFAM, showing the logarithm of the amplitude computed from 60 minutes of Hα velocity data for the 1, 3, 5, and 7 mHz frequency bands, from left to right. The top (bottom) row shows the amplitude in the flare region FR_1 (FR_2) from segments centered at about 9 and 23 minutes after flare initiation, respectively. The color scale is clipped at 0.5 of the maximum velocity amplitude to emphasize smaller scale features.

(Animations of this figure are available in the online journal.)

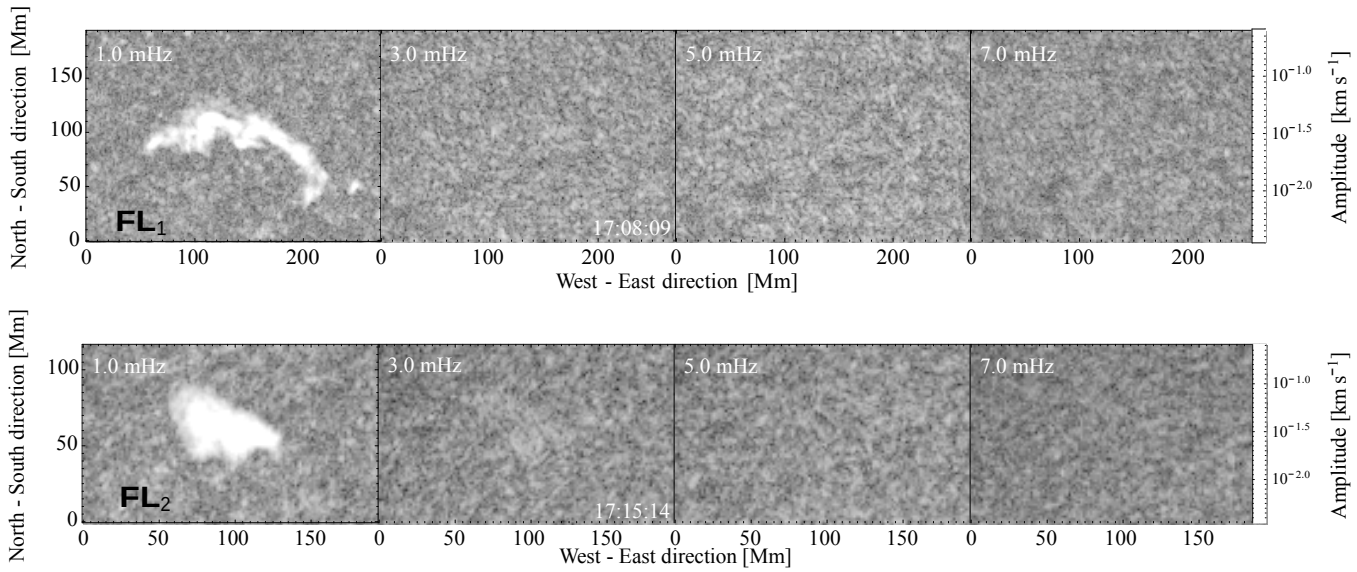

Figure 3. Filaments during the 2005 May 13 flare. Each panel is a snapshot of an FFAM, showing the logarithm of the amplitude computed from 60 minutes of Hα velocity data for the 1, 3, 5, and 7 mHz frequency bands, from left to right. The top (bottom) row shows the amplitude in two quiescent filament regions FL_1 (FL_2) for each frequency passband, about 55 and 62 minutes after flare eruption, respectively. The color scale is clipped at 0.5 of the maximum velocity amplitude.

(Animations of this figure are available in the online journal.)

To produce the FFAMs, consider a general data cube (we will be working with intensity and Doppler velocity) of two spatial and one temporal dimensions, $\boldsymbol{f}(x, y, t)$. Assume that there are N time steps (images) available. For each time step t_i, the following steps are carried out.

1. Filter the data in the time domain over a segment of length T, which in this study is always taken to be 60 minutes, thus comprising $N_T = 60$ images. The 60 minute filter tapers off quickly, but smoothly to zero at each "edge." In other words, only the subsequent N_T images after the current time step are considered. The filtering is represented as

$$\boldsymbol{f}_i(x, y, t; T) = F_1(t; [t_i, t_i + T]) \cdot \boldsymbol{f}(x, y, t), \quad (1)$$

where the brackets in the second argument of the filter F_1 denote the range where it is nonzero and equal to unity. The

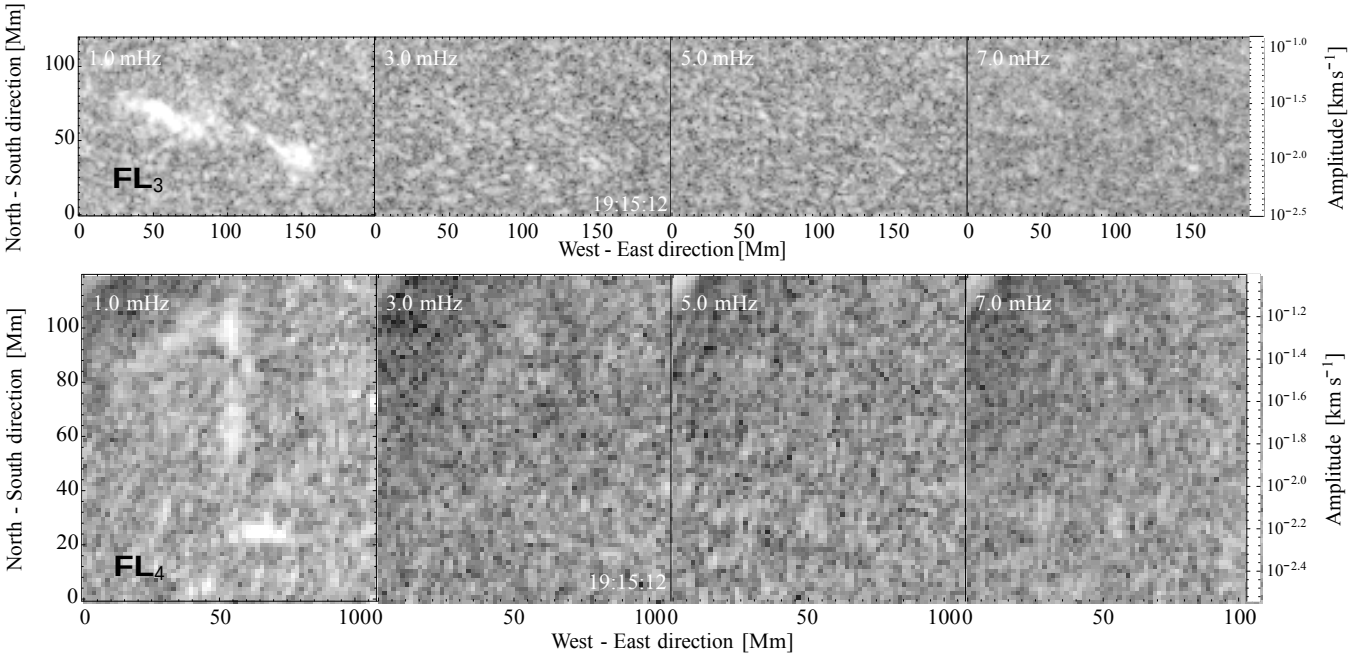

Figure 4. Filaments during the 2006 December 6 flare. Each panel is a snapshot of an FFAM, showing the logarithm of the amplitude computed from 60 minutes of Hα velocity data for the 1, 3, 5, and 7 mHz frequency bands, from left to right. The top (bottom) row shows the amplitude in two quiescent filament regions FL_3 (FL_4) for each frequency passband, about 35 minutes after flare eruption. The color scale is clipped at 0.5 of the maximum velocity amplitude.

(Animations of this figure are available in the online journal.)

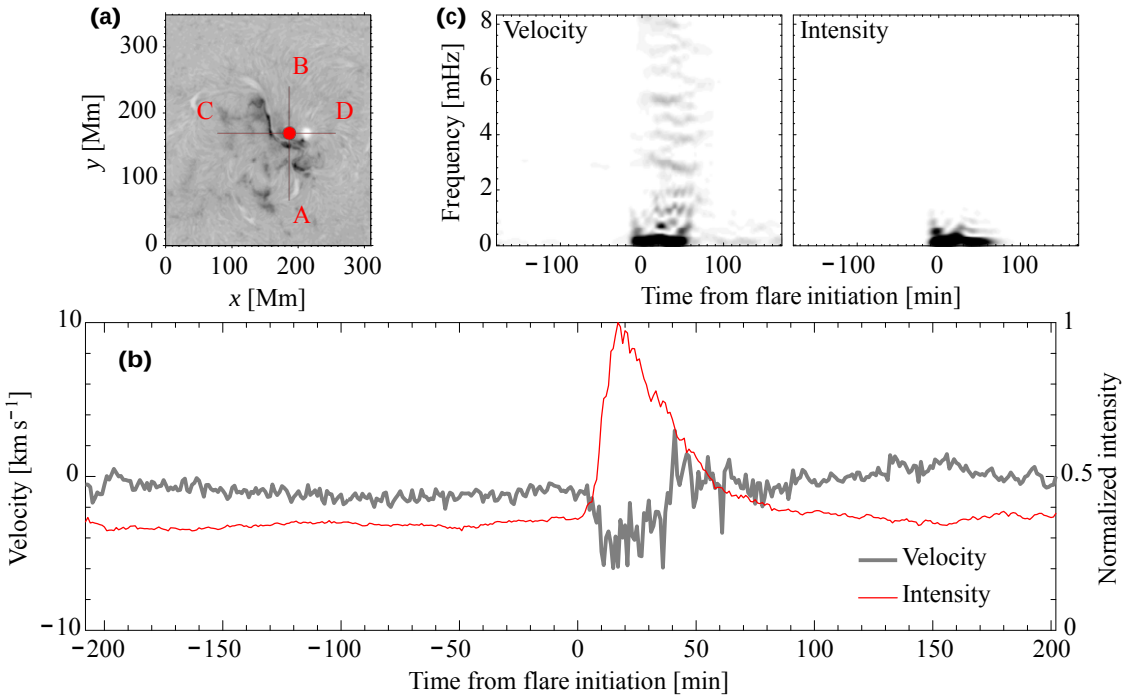

Figure 5. Analysis of flare FR_1 using standard methods. (a) A snapshot of intensity around the flare. The red circle indicates the pixels (radius of 10 pixel) that were averaged to compute the time series in panel (b). The horizontal and vertical lines denote slices used for the plots in Figure 6. (b) Time series of normalized intensity and Doppler velocity for the set of pixels in the flare region as a function of time. (c) Wavelet power spectra of the velocity and intensity light curves from (b). The (linear) gray scale in these plots is such that black denotes higher signal, and has been clipped to half of the maximum power to emphasize details.

(A color version of this figure is available in the online journal.)

filtered data $\overline{f}_i$ are labeled by the particular starting time step i and the segment length T.

2. Compute the temporal power spectrum of that segment

$$P_i(x, y, \nu; T) = \left| \sum_{i=1}^{N_T} \overline{f}_i \exp(2\pi i \nu t_i) \right|^2 , \qquad (2)$$

where ν is the cyclic frequency. Only the data over the segment T will contribute to the power. We subsequently convert this power spectrum to an amplitude spectrum $A_i(x, y, \nu; T)$ to get units of velocity when using Doppler velocity data.

3. Apply a second filter F_2 in frequency to the amplitude spectrum, which has a central frequency ν_0 and a bandwidth

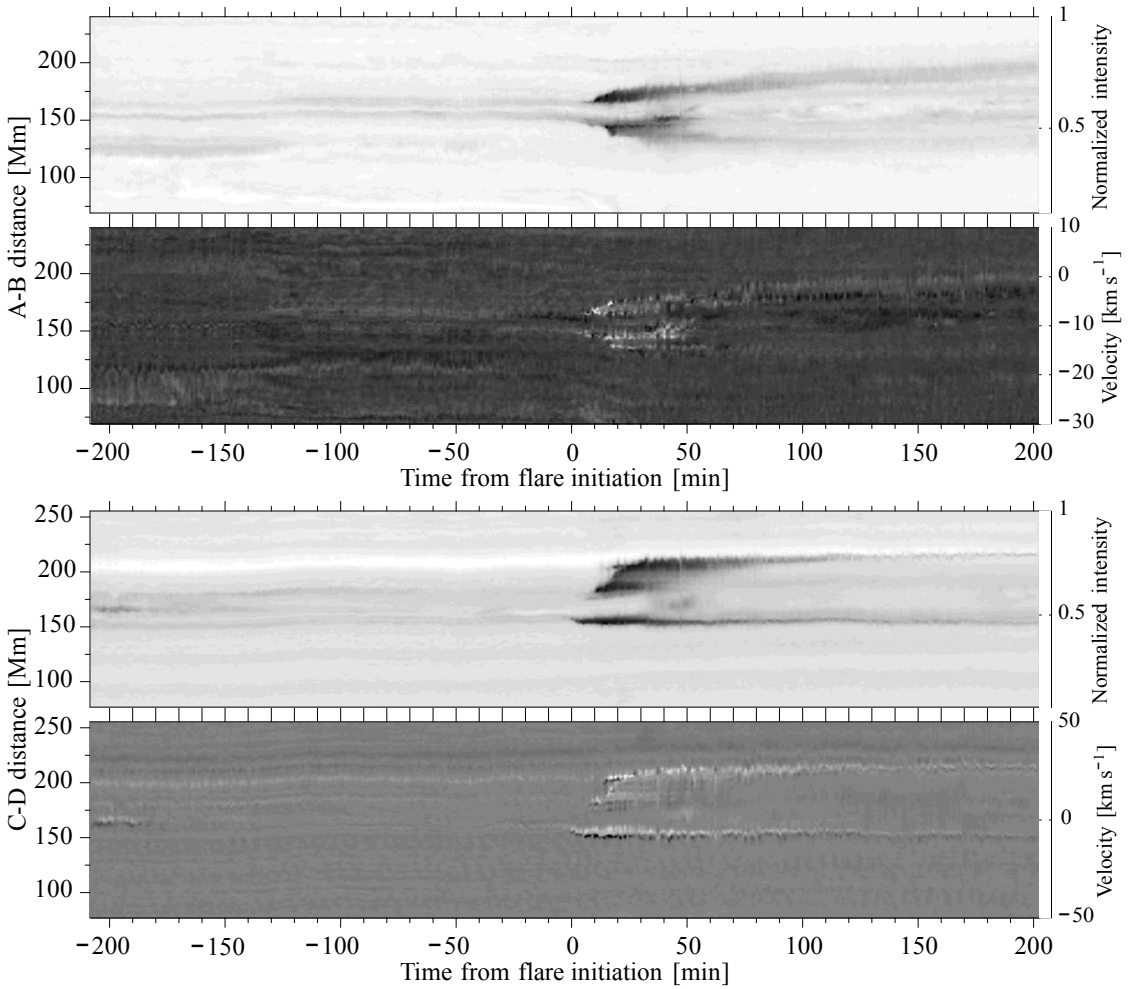

Figure 6. Stack plots of flare FR_1 along the slices indicated in Figure 5(a). The top two panels show the intensity and velocity time dependence along the A–B vertical line through the flare. The bottom two panels show the intensity and velocity time dependence along the C–D horizontal line through the flare.

of $\Delta\nu$, and compute the average over the frequencies in that particular band:

$$\overline{A_i}(x, y; \nu_0, \Delta\nu, T) = \left(F_2(\nu; \nu_0 \pm \Delta\nu/2)\, A_i(x, y, \nu; T)\right)_\nu, \quad (3)$$

where the $(\ldots)_\nu$ operator indicates an average over the values of frequency in the range $\nu_0 \pm \Delta\nu/2$. The amplitude quantity $\overline{A_i}$ is a 2D image labeled by central frequency, bandwidth, and segment length.

4. Continue for all i :($N - N_T$ (the final T minutes are not computed to avoid the "edge"). The final data product, FFAM = $\bigcup_i \overline{A_i}$, is a 3D quantity in x, y, t. It can be visualized as a movie (see online examples).

We consider frequencies in 1 mHz wide bands, centered on the values ν_0 = 1, 3, 5, and 7 mHz. The temporal Nyquist frequency for the ISOON cadence is 8.3 mHz. The data sets in this study are approximately 420 minutes in length. Since segments from which we compute the amplitude spectrum are only 60 minutes in length, the frequency sampling is $d\nu \sim 0.28$ mHz. Therefore, the average over each 1 mHz band uses about 3–4 images. We have performed experiments with shorter and longer T, as well as with different bandwidths and central frequencies, and the results are qualitatively similar to those shown in Section 4.

4. RESULTS

We compute and study FFAMs of the oscillatory dynamics associated with the ISOON flaring events at different frequencies, and discuss the active region oscillations and the filament oscillations separately.

4.1. Oscillations in Flare Regions

The active regions in which the flares occur in the 2005 and 2006 events show oscillatory features over the entire frequency range studied here. The likelihood of a strong contribution from the underlying photospheric acoustic p modes can be ruled out for several reasons. The dramatic increase in amplitude occurs only once the flare erupts. If the p modes were responsible, then their effects would be present over the entire data sequence. Second, the frequency range considered here is mostly below the photospheric acoustic cutoff frequency (~5.3 mHz). The filter bandpass of ISOON is also quite narrow, much more so than the instrument used by Harvey et al. (1993), where both 5- and 3-minute oscillations were seen in Hα. We are confident that the effects studied here are confined mostly to the chromosphere.

Figure 2 shows oscillations as a function of frequency in one snapshot of the FFAM from velocity data for flare regions FR_1 and FR_2. The central time of the 60 minute segment used in the computation is provided. The figures represent the slice at the

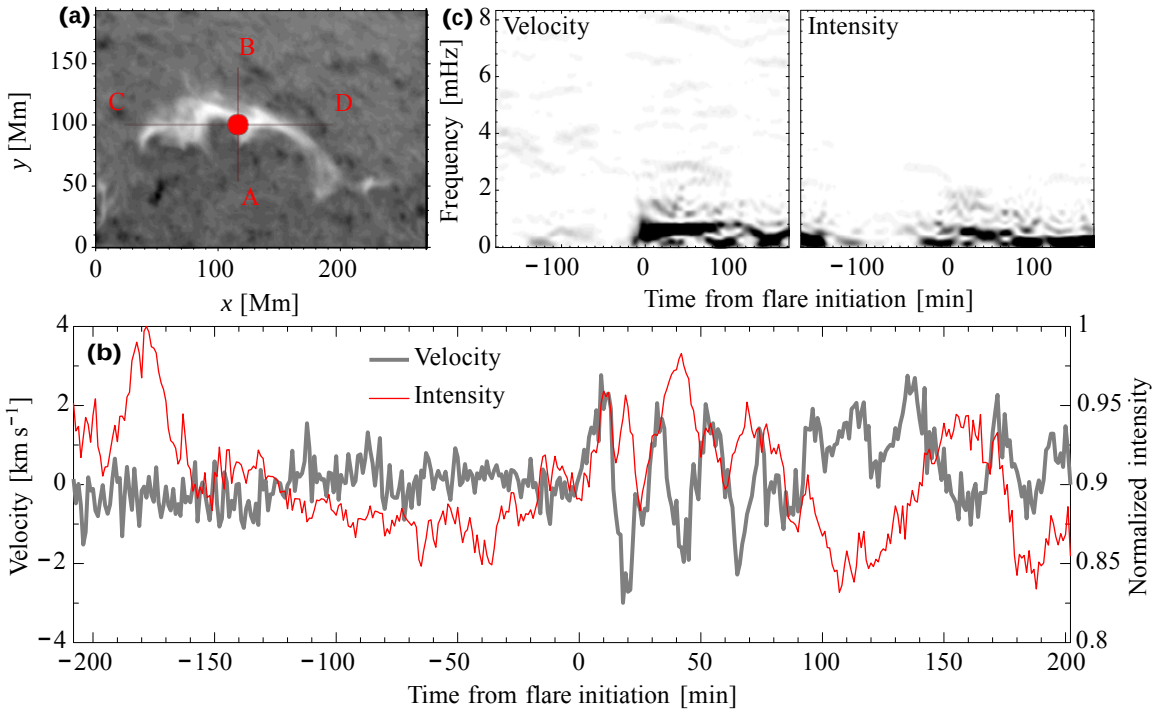

Figure 7. Analysis of filament FL_1 using standard methods. (a) A snapshot of intensity around the filament. The red circle indicates the pixels (radius of 10 pixel) that were averaged to compute the time series in panel (b). The horizontal and vertical lines denote slices used for the plots in Figure 8. (b) Time series of normalized intensity and Doppler velocity for the set of pixels in the filament region as a function of time. (c) Wavelet power spectra of the velocity and intensity light curves from (b). The (linear) gray scale in these plots is such that black denotes higher signal, and has been clipped to half of the maximum power to emphasize details.

(A color version of this figure is available in the online journal.)

maximal amplitude of the time series. For FR_1, the UT 16:22 moment is about 9 minutes after the flare erupted. Thus, there is both pre- and post-flare signal in the derived amplitude. For FR_2, the 18:17 slice is about 23 minutes before the flare erupted; thus, there is mostly pre-flare signal involved in the computation.

It is evident from the figure that the flares "excite" all of the frequencies from about 0.5 to 7.5 mHz to detectable amplitudes in velocity (note that the figure is on a logarithmic scale). We are unaware of any previous studies that demonstrate this. The velocities in the 1 mHz band reach about 3 km s^{-1} and 4 km s^{-1} at peak amplitude for the 2005 and 2006 data, respectively, and are usually reduced at higher frequencies. The stronger amplitudes in FR_2 could be due to the fact that it is near the limb, thus implying stronger horizontal motions. Interestingly, the 2006 flare's maximal amplitude is in the 3 mHz band, at about 5 km s^{-1}. In intensity, the higher frequencies near each flare contribute much less oscillatory power, as is discussed further in Section 4.3.

Once the flare erupts, the excess oscillatory amplitude lasts for about 100 minutes after the peak in the FFAM, although this strongly depends on the location near the ribbons. Some regions are damped much faster or more strongly than others. Due to the 60 minutes time-averaging involved in creating the FFAMs, it is not convenient to determine the precise duration of the increase in oscillation amplitude, as the time resolution is insufficient to give certainty to this number. More spatial structure is seen in the 1 mHz band, especially in the plage area of the active regions, and the two flare ribbons in FR_1 are somewhat visible in the oscillation amplitudes, as is the sunspot on the northern edge. FFAMs were computed using the ISOON Hα line core (intensity) data as well, and the same general spatial characteristics are seen, except for weaker power at high frequencies.

4.2. Low-frequency Oscillations in Filaments

Throughout these two data sets, the solar disk was littered with quiescent filaments. We identify and analyze two of them for each event, denoted by FL_{1-4}. The FFAMs show a very dramatic "lighting up" (a rapid increase in oscillation amplitude) of the filaments well after the distant flares erupt, although each event has somewhat different characteristics.

Figure 3 shows snapshots from the FFAM of filaments FL_1 and FL_2 in the 2005 time series. The images are those where the filament oscillation amplitude peaks in the FFAM, corresponding to the time segment centered at 55 and 62 minutes after the flare erupts for FL_1 and FL_2, respectively. One explanation of the different timings is that the filaments are at different distances from the flare center (see Figure 1), and whatever activation mechanism is at work (such as a chromospheric wave) needed to travel different distances.

The noticeable difference compared to the oscillations in the flare region is that the filament only shows strong amplitude excess in the lowest frequency bandpass of 1 ± 0.5 mHz, even on the logarithmic scale. This corresponds to periods in a range from about 11 to 33 minutes. The amplitude is significantly above the background level in this passband, lasting for about 100 minutes. The velocities of the oscillations are on the order of 0.5–1.0 km s^{-1}. This is the first detection of oscillatory behavior in these two particular filaments.

As in previous studies (Tripathi et al. 2009), one might conclude that anywhere from about 3 to 10 periods of the filament oscillation took place after it was excited. With our method, it may be too simplistic to make such a conclusion, since there are small-scale spatial structures that are operating on different timescales, as is clearly evident in the FFAMs. Some regions show low-frequency power for the whole duration (like

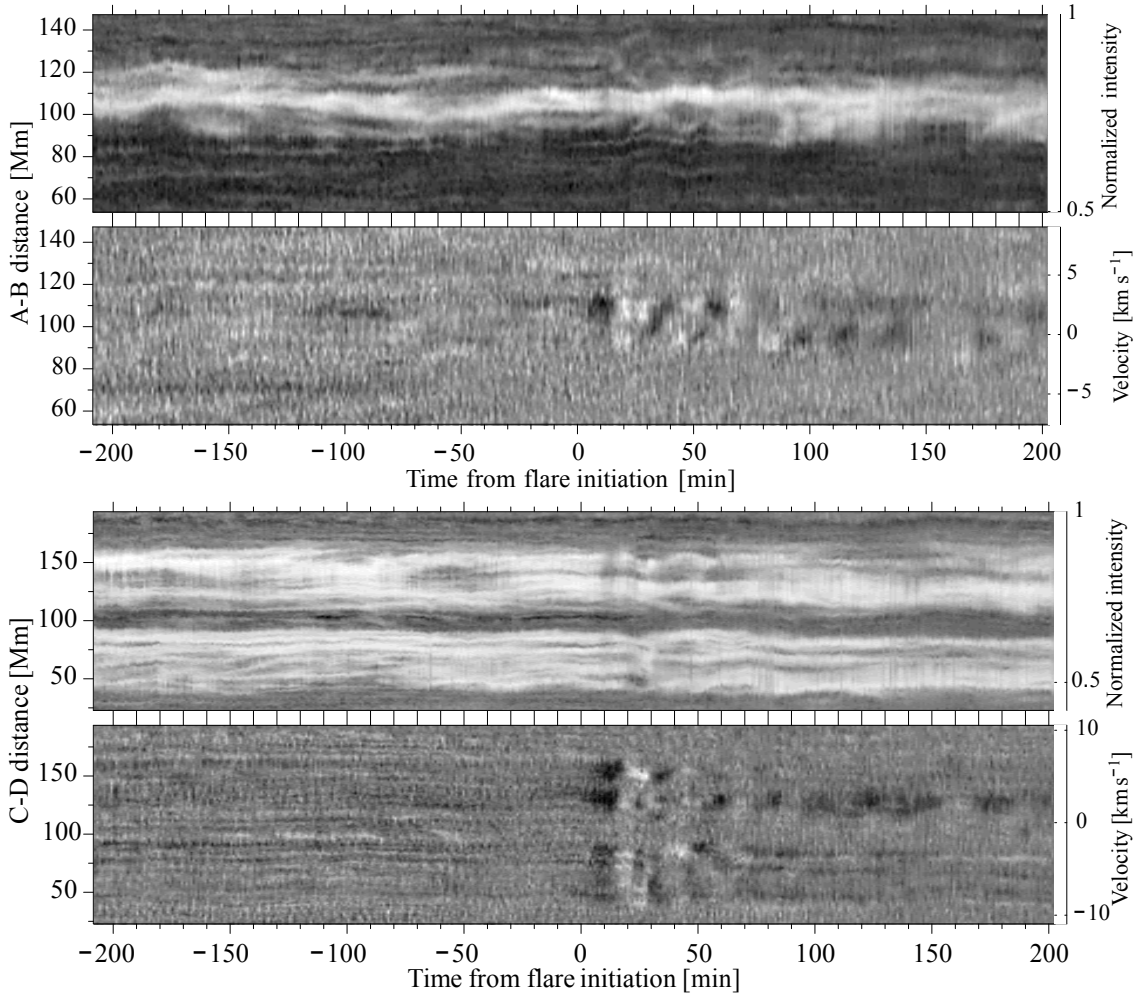

Figure 8. Stack plots of filament FL_1 along the slices indicated in Figure 7(a). The top two panels show the intensity and velocity time dependence along the A–B vertical line through the filament. The bottom two panels show the intensity and velocity time dependence along the C–D horizontal line through the filament.

the central part of the filament), while others do not (the "ends" of the filament).

The 2006 quiescent filaments are shown in Figure 4. We note again that a strong Moreton wave was associated with this flare that propagated outwardly from the active region at speeds up to 1600 km s^{-1} (Balasubramaniam et al. 2010). The wave passed near both filaments and presumably activated their oscillations. The maximum values of the amplitudes in this case are ≈0.2 km s^{-1}, less than half the strength than was found in the FL_1 and FL_2 filaments. Filament FL_3 shows no oscillations in its center, only on its ends, which is a curious feature. Additionally, even though these two filaments are not equidistant to the flare region, the maximal oscillation amplitude occurred at approximately the same time.

That the velocity oscillation signal in the filaments is weaker than in the 2005 event is surprising, given that there is a clear and strong Moreton wave observed that interacts with the filaments. Possible explanations for this discrepancy might include viewing geometry, intrinsic difference in filament properties, lower quality of data, or the overall distance of the filaments from the flare, which is larger than in the 2005 case.

4.3. Comparison of Method to Other Analysis Techniques

Analyzing 1D time series of various regions by wavelet analysis is one technique that has become standard for the study of filament oscillations (e.g., Pintér et al. 2008). Computing "stack plots" of the signal along a certain slice of the data as a function of time is another (e.g., Li & Zhang 2012). We carry out such analyses to compare and contrast the results with those of the FFAMs for the flare FR_1 and filament FL_1 regions. The other regions show similar behavior.

Figure 5 shows an analysis of FR_1. A set of pixels near the flare ribbons was averaged and time series of intensity and velocity were obtained. The intensity light curve shows the characteristic flare impulse and exponential decay, accompanied by low-level oscillations, while the velocity shows a fluctuating signal on top of a sudden blueshift (toward observer) as the flare erupts. Other pixels in the flare-ribbon region show redshifts at flare onset (for a detailed discussion of velocity profiles in broadband Hα measurements, see Ichimoto & Kurokawa 1984). In both cases, the frequency content of the oscillations is difficult to quantify in the time series alone. Wavelet analysis of this set of pixels confirms that all of the frequencies in velocity are activated, but that the low frequencies are strongest, as the FFAMs indicated. The strongest amplitudes last for about 80 minutes. The spectrum in intensity does not show much high-frequency power. These conclusions change somewhat as different regions are analyzed.

Perpendicular slices through the flare ribbons passing through the center of the same set of pixels are used to produce stack plots for intensity and velocity and are given in Figure 6. From the horizontal slice, one sees that the east side of the flare (closest

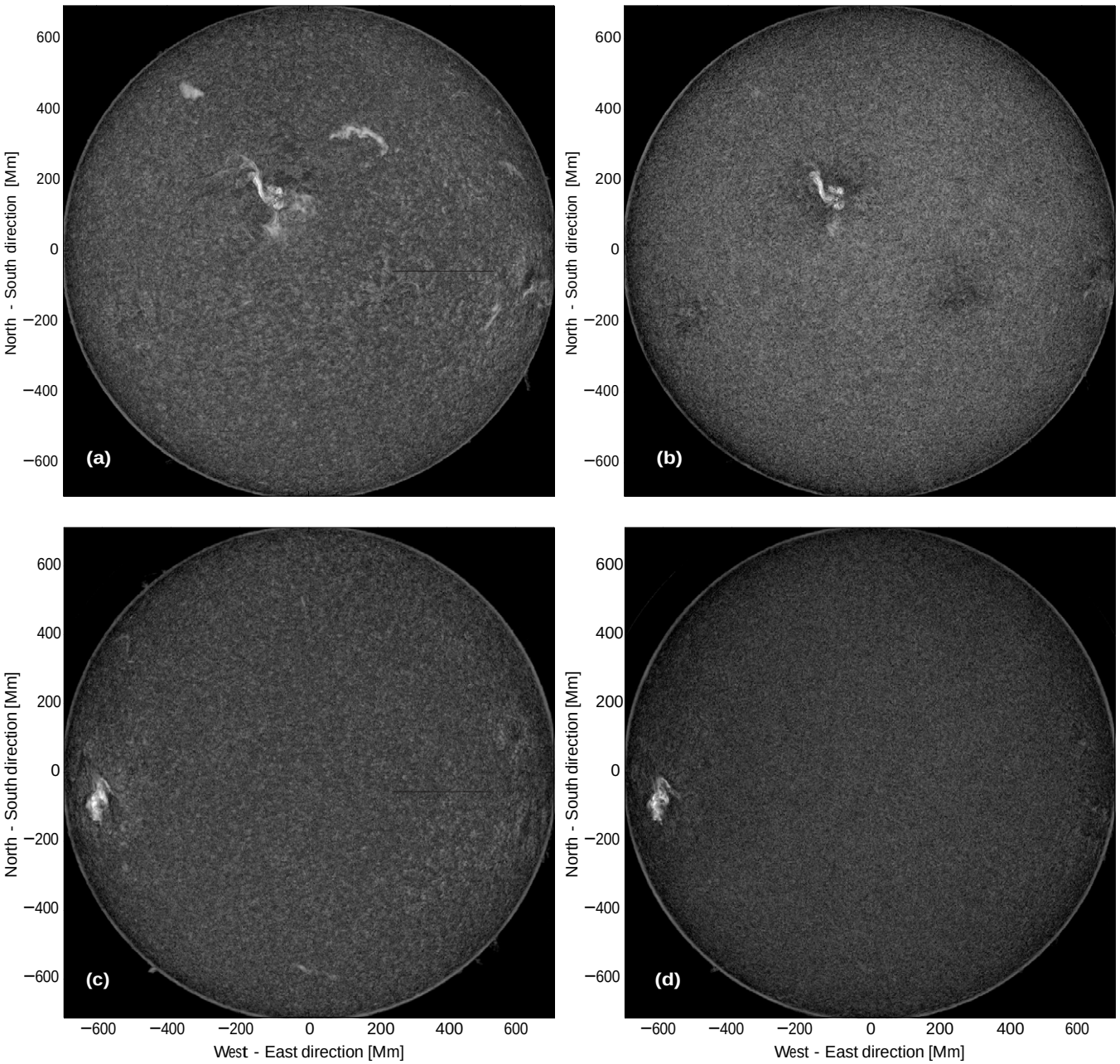

Figure 9. Snapshots of full-disk velocity FFAMs around peak flare intensity. Panels (a) and (b) are the 1 mHz and 3 mHz bands for the 2005 flare, respectively. Panels (c) and (d) are the 1 mHz and 3 mHz bands for the 2006 flare, respectively. All panels are plotted on the same gray scale.

(Animations of this figure are available in the online journal.)

to point C) is the first to begin oscillating, as is also evident in the FFAM. The strongest signal comes from the outer edge of the ribbons. The velocity stack plots indicate that the east–west direction (C–D) has a higher signal-to-noise ratio, even though the other direction has the larger overall amplitude.

Figure 7 shows a similar analysis for the filament FL_1. A set of pixels near the center of the filament that showed strong oscillations in velocity was chosen and averaged to give the time series. There are 6–7 long-period oscillations ($\sim$20 minutes) at amplitudes of about 1 km s^{-1} in this region, and these show up clearly in the wavelet spectra. In intensity, the variations in the time series are less well defined, but the wavelet spectra do reveal the low-frequency nature of the oscillations. Contrasting with the chosen flaring region, the strong amplitudes near the filament persist for well over 100 minutes. The stack plots in Figure 8 show slices through the filament along perpendicular directions. Again, the global view of the intensity slice is not particularly useful for studying any variations, while the velocity plots clearly show the filament being triggered by the flare and its subsequent oscillations. The motion appears to be primarily in the east–west longitudinal direction.

The use of these standard techniques is indeed very useful for studying these phenomena, especially when coupled with an analysis using FFAMs. However, the choice of pixels and slice coordinates to produce Figures 5–8 requires a lot of trial and error, and the inferences vary strongly from region to region. This could be expedited by first using the FFAMs to choose suitable regions that show interesting behavior, and then looking

into more detail with the other methods. It is interesting that the stack plots in intensity for the filament do not strongly show the flare eruption, at least along these particular slices, while the intensity FFAMs and wavelets clearly do.

4.4. Summary of Results

To summarize the analyses, we observe the fascinating occurrence of rapid communication at large distances across the solar disk. In the 2005 event, strong amplitude increases on the far western solar limb are observed, very far from the flare area in the eastern hemisphere. Indeed, Figure 9 shows full-disk snapshots of velocity FFAMs in the two lowest bandpasses near the peak flaring times. The filamentary amplitudes are evident everywhere at low frequency, and rather absent at 3 mHz and higher. For the 2006 flare, the 1 mHz band shows weak excess acoustic power just outside the flare region, and one barely discerns the brightenings in filaments FL_3 and FL_4 in this global picture.

A comparison with other large-amplitude filament oscillations as reviewed by Tripathi et al. (2009) and Arregui et al. (2012) is useful. Other published studies find oscillations with minimum amplitudes near 20 $km\,s^{-1}$. In line-of-sight velocity images from the Polarimeter for Inner Coronal Studies (PICS) Hα instrument, Gilbert et al. (2008) find that the FL_3 filament oscillates at amplitudes up to 41 $km\,s^{-1}$. We find amplitudes of a few $km\,s^{-1}$ in the flare regions themselves, but less than 1 $km\,s^{-1}$ in the filaments at low frequency. In the raw Doppler signal from ISOON, we find maximum velocities of the FL_3 filament of several $km\,s^{-1}$.

While we do observe features that approach several tens of $km\,s^{-1}$ in the line-of-sight velocity data, particularly in the flare (see Figure 6, for example), the coherent variations over an extended time period do not possess such amplitudes. We attribute the discrepancy with other values in the literature to the fact that the FFAMs select out the persistent variations over longer timescales (in the computations here, at least 60 minutes), and thus it is a matter of effective time resolution. Differences in instrumentation likely have some effects too.

For filament oscillation periods, studies have found a range from about 6 to 150 minutes (Tripathi et al. 2009). The periods found here are on the lower end of those values, but still consistent with them. One might argue that small-amplitude oscillations are a suitable classification for these events, which tend to have a few $km\,s^{-1}$ amplitudes, but can also have very short periods on the order of seconds to a few minutes, which we are unable to observe.

Gilbert et al. (2008) have already studied both FL_3 and FL_4 using different data and standard methods. For FL_3, they find 3 hr of oscillatory motions, somewhat longer than found here by about 30 minutes. They also find periods from 18 to 39 minutes. For FL_4, they find the duration of oscillations to be only about 17 minutes, whereas we observe increased power (at 1 mHz) for more than 1 hr. The different diagnostics as a function of frequency is an advantage of the method presented here.

5. DISCUSSION

This work is important for two reasons: (1) we have presented a simple algorithm for both visualizing and studying dynamic phenomena in 2+1 dimensions with differing frequency content; and (2) we have used this technique to analyze two different events that exhibit low-frequency filament oscillations excited by a distant flare. We observe robust oscillations in the active regions where the flares erupt over a broad range of frequencies. Photospheric modes can be ruled out as the source since the oscillation amplitude only increases after the flare initiates.

Strangely, the weaker filament oscillations are observed in the system that interacted with a strong Moreton wave, which can trigger of such oscillations, but it is possible that line-of-sight effects or wave propagation direction can be involved in these differences. The velocities found in the FFAM analysis do not fit into the large- and small-amplitude oscillation classifications. It might be useful to have sub-categories of such events that show oscillating strengths as a function of frequency. We have been able to confirm the work of Gilbert et al. (2008), who showed that the FR_4 filament is a lower-amplitude oscillator than the other filament in the 2006 December flare event.

The spatial features of the velocity power in the different frequency bands show interesting dynamics, particularly for the filaments. We observe different sections of the filaments fluctuating over various timescales, indicating that either the damping of the oscillations is spatially dependent, or the excitation is not constant over the entire length of the filaments, or some combination of both effects. More detailed analysis of this is underway.

There is both new and complementary information when comparing the original full-disk time series and the FFAMs (the movies associated with Figure 1 and the FFAMs of Figure 9). For example, for the 2005 event, in the raw intensity time series, one clearly sees the reaction of some of the far-away filaments after flare eruption, but the FFAM indicates that some filaments are actually not affected by the (unknown) trigger mechanism, and also directly provides the oscillation frequencies of those which are. In the 2006 flare, the Moreton wave is easily visible in both intensity and Doppler data, yet the response of the filaments is rather muted when viewed in the FFAM, suggesting that the oscillation activation was not as effective. Certainly, more events need to be treated in such a systematic fashion to understand if these are common occurrences or not.

We finally point out that at the photosphere, active regions typically show an enhancement of acoustic power at *higher* frequencies, known as acoustic halos (Braun et al. 1992). This is quite different than the case here, where we see higher amplitudes in the lower-frequency bandpasses. Knowing how the frequency content of waves changes through the different layers of the atmosphere could help in understanding the local environment parameters that are quite difficult to directly observe, such as magnetic field and density. EUV waves can also presumably interact with filaments, although for the two events studied here there were no EUV data that could be used to identify any such contribution. In the future, this method will be used to study a range of various chromospheric data.

We acknowledge fruitful conversations with Stuart Jefferies, Michael Kirk, Frank Hill, and R. T. James McAteer. This work was supported in part by an NSF PAARE award AST-0849986.

REFERENCES

Arregui, I., Oliver, R., & Ballester, J. L. 2012, LRSP, 9, 2
Asai, A., Ishii, T. T., Isobe, H., et al. 2012, ApJL, 745, L18
Balasubramaniam, K. S., Christopoulou, E. B., & Uitenbroek, H. 2004, ApJ, 606, 1233
Balasubramaniam, K. S., Cliver, E. W., Pevtsov, A., et al. 2010, ApJ, 723, 587
Balasubramaniam, K. S., Pevtsov, A. A., & Neidig, D. F. 2007, ApJ, 658, 1372
Bisi, M. M., Breen, A. R., Jackson, B. V., et al. 2010, SoPh, 265, 49
Braun, D. C., Lindsey, C., Fan, Y., & Jefferies, S. M. 1992, ApJ, 392, 739

Elliott, I. 1969, SoPh, 6, 28
Eto, S., Isobe, H., Narukage, N., et al. 2002, PASJ, 54, 481
Gilbert, H. R., Daou, A. G., Young, D., Tripathi, D., & Alexander, D. 2008, ApJ, 685, 629
Harvey, J. W., Duvall, T. L., Jr., Jefferies, S. M., & Pomerantz, M. A. 1993, in ASP Conf. Ser. 42, GONG 1992. Seismic Investigation of the Sun and Stars, ed. T. M. Brown (San Francisco, CA: ASP), 111
Ichimoto, K., & Kurokawa, H. 1984, SoPh, 93, 105
Isobe, H., & Tripathi, D. 2006, A&A, 449, L17
Jain, R., & Tripathy, S. C. 1998, SoPh, 181, 113
Kazachenko, M. D., Canfield, R. C., Longcope, D. W., et al. 2009, ApJ, 704, 1146
Li, T., & Zhang, J. 2012, ApJL, 760, L10
Liu, C., Lee, J., Yurchyshyn, V., et al. 2007, ApJ, 669, 1372
Maurya, R. A., & Ambastha, A. 2008, JApA, 29, 249
Neidig, D., Wiborg, P., Confer, M., et al. 1998, in ASP Conf. Ser. 140, Synoptic Solar Physics, ed. K. S. Balasubramaniam, J. Harvey, & D. Rabin (San Francisco, CA: ASP), 519
Okamoto, T. J., Nakai, H., Keiyama, A., et al. 2004, ApJ, 608, 1124
Pintér, B., Jain, R., Tripathi, D., & Isobe, H. 2008, ApJ, 680, 1560
Ramsey, H. E., & Smith, S. F. 1966, AJ, 71, 197
Tripathi, D., Isobe, H., & Jain, R. 2009, SSRv, 149, 283
Vršnak, B., Veronig, A. M., Thalmann, J. K., & Žic, T. 2007, A&A, 471, 295
Yurchyshyn, V., Liu, C., Abramenko, V., & Krall, J. 2006, SoPh, 239, 317

DISTRIBUTION LIST

DTIC/OCP
8725 John J. Kingman Rd, Suite 0944
Ft Belvoir, VA 22060-6218 1 cy

AFRL/RVIL
Kirtland AFB, NM 87117-5776 2 cys

Official Record Copy
AFRL/RVBXS/Karatholuvu Balasubramaniam 1 cy

This page is intentionally left blank.